A novel, low-cost technique for modeless calibration of a 3-DoF PKM

Bence TIPARY[a, b], Gábor ERDŐS[a,b]

[a] *Institute for Computer Science and Control (SZTAKI), Eötvös Loránd Research Network (ELKH), Budapest, Hungary*
[b] *Department of Manufacturing Science and Engineering, Budapest University of Technology and Economics, Budapest, Hungary*

Contact information:
Bence Tipary (corresponding author): bence.tipary@sztaki.hu
Gábor Erdős: gabor.erdos@sztaki.hu

Abstract

Purpose

The purpose of this paper is to propose a novel measurement technique and a modeless calibration method for improving the positioning accuracy of a 3-DoF parallel kinematic machine (PKM). The aim is to present a low-cost calibration alternative, for small and medium-sized enterprises (SMEs), as well as educational and research teams, with no expensive measuring devices at their disposal.

Design/methodology/approach

Using a chessboard pattern on a ground-truth plane, a digital indicator, a 2D eye-in-hand camera and a laser pointer, positioning errors are explored in the machine workspace. With the help of these measurements, interpolation functions are set up per direction, resulting in an interpolation vector function to compensate the volumetric errors in the workspace.

Findings

Based on the proof of concept system for the linear-delta PKM, it is shown that using the proposed measurement technique and modeless calibration method, positioning accuracy is significantly improved using simple setups.

Originality/value

In the proposed method, a combination of low-cost devices is applied to improve the 3D positioning accuracy of a PKM. By using the presented tools, the parametric kinematic model is not required, furthermore the calibration setup is simple, there is no need for hand-eye calibration and special fixturing in the machine workspace.

Keywords

Parallel kinematic machine, Calibration, Error compensation

1. Introduction

In traditional robotic applications, robot accuracy requirements are not strict, since the points or paths to be traced are set-up manually to properly meet the specifications. These robot tasks are taught under the same environmental conditions as during operation. However, there is an increasing demand for offline robot programming related robot applications, where absolute accuracy is of key importance. For such tasks, robot calibration is inevitable, which in most cases aims to improve robot accuracy through software, rather than prescribing tight manufacturing and assembly tolerances or modifying the mechanical structure (Nubiola, 2014).

Robot calibration methods can be classified to model-based and modeless approaches. Model-based methods consist of four steps: establishing the parametric kinematic model of the robot, measurement of robot poses, identification of the model parameters and error compensation (Mooring *et al.*, 1991).

On the other hand, modeless calibration methods do not need a parametric error model, and compensation is realized using interpolation techniques. In this case, the workspace is discretized to a grid, and measurement is carried in each gridpoint. The pose error of the end-effector is compensated based on the neighboring gridpoints (Zhuang and Roth, 1996). While this technique requires much more measurement points, the calibration process itself is simpler, and the achievable improvement is greater than in case of model-based approaches. The use of the model-based method is limited to the (mostly geometrical) error sources included in the model, however in the modeless case, the errors are explicitly measured and compensated.

This paper proposes a novel technique for modeless calibration of a parallel kinematic machine (PKM). Using a digital indicator, an eye-in-hand camera, a laser pointer and a chessboard pattern, 3D positioning errors can be compensated in the workspace in a local fashion, wherever task execution needs to be carried out.

Calibration is a widely researched topic, and many different solutions are proposed for different scenarios. A combined model-based and modeless calibration approach was presented by Guo *et al.*, 2015 for serial industrial robots, to compensate geometric and non-geometric errors. Other papers propose non-parametric approaches, where the robot kinematic parameters are not modified during the calibration, instead the modification is made in the controller command (Cai *et al.*, 2018; Cao *et al.*, 2019; Patel *et al.*, 2019). Online error compensation is a further possibility, which utilizes servoing techniques to improve accuracy (Jiang *et al.*, 2016).

Chessboard pattern as a calibration instrument is commonly used for camera calibration, i.e., determining the camera's intrinsic or even extrinsic parameters (De la Escalera and Armingol, 2010). However, it can also be applied for vision system-based robot calibrations (Li *et al.*, 2017; Meng and Zhuang, 2007; Özgüner *et al.*, 2020).

There are a number of studies focusing on PKM calibration. A combined parametric and non-parametric calibration approach for a PKM is presented in Liao *et al.*, 2020, to tackle geometric and non-geometric errors. In Wang and Bai, 2012, a neural network based modeless calibration method is proposed for a Stewart platform. (Dehghani *et al.*, 2014) presented a chessboard pattern and camera-based approach. Further calibration techniques applied to PKMs are reviewed in Majarena *et al.*, 2010 and Mekid and Ogedengbe, 2010. Although the majority of approaches in the literature are at least partially model-based ones, due to their smaller workspace volumes, PKMs are much more suitable for modeless calibration than serial robots.

Calibration in the industry is often performed using expensive measuring devices such as laser trackers, precise stereo camera systems or calibration instruments with an intricate setup (Nubiola, 2014). Eye-in-hand vision systems need to be rigidly attached to the robot end-effector and require hand-eye calibration. Moreover, the calibration process often requires manual operations with trained personnel. Also, in case of model-based calibration, the parametric kinematic model needs to be set up in a similar form as in the machine controller, and the parameters need to be refined and updated in the controller in order to improve the accuracy.

The proposed approach aims to provide a reasonable calibration alternative using low-cost devices and simple setups. This method can be beneficial for small and medium-sized enterprises (SMEs), educational and research teams, who cannot afford expensive measurement devices for calibration purposes or may not have skilled workforce for any of the traditional model-based calibration steps (e.g., establishing the error model or performing measurement).

The novelty of the method is the application of a combined measurement system to realize a two-step calibration process. First, by scanning the top surface of the worktable (or a parallel reference plane) with the help of a digital indicator, the positioning errors along the axis perpendicular to the plane are determined and compensated. Then, using a chessboard pattern and a laser-camera system attached to the end-effector, the in-plane deviations are measured and compensated as well.

Unlike most chessboard pattern application, here, this reference is not used for hand-eye calibration, but for measuring the projection of the virtual tool axis (represented by a laser beam) in order to determine its location in the plane. In fact, no hand-eye calibration is required, as by using a calibrated pin-hole type camera, the perspective distortion of the images is overcome by homography transformation, based on the ground-truth chessboard pattern. Cameras fixed on robot links tend to displace due to cable stretching, thermal effects or loosening of fasteners, which cause inaccurate hand-eye configuration and require regular calibration. The proposed approach reduces the burden of having a rigidly fixed camera with a precisely known relation w.r.t. the end-effector. Moreover, apart from the calibration setup, the measurement, evaluation and compensation processes are all automated. The proposed method is applicable for machines with small workspace volumes, as well as local calibration, if tasks are carried out in smaller, limited local spaces.

2. Methodology

The proposed modeless approach consists of two steps. First, levelling is performed in the z-axis using a digital indicator on the worktable. Then, the planar error compensation is carried out with a vision-laser system and a chessboard pattern. In the very beginning, the mathematical formulations are summarized.

It is typical to send task space ($\boldsymbol{r} = (x, y, z)$) commands to PKM controllers instead of joint space ones ($\boldsymbol{q} = (q_1, q_2, q_3)$), since these are easier to interpret for engineers. Task space coordinates are defined in a common machine reference frame (see later, in Figure 3), including both digital (i.e., on the controller side) and physical positions ($\boldsymbol{r^d}$ and $\boldsymbol{r^p}$, respectively). The digital positions are considered nominal, and are used during planning.

Then, these are part of the commands sent to the controller. The digital task space positions ($\boldsymbol{r^d} = (x^d, y^d, z^d)$) are transformed to joint pose commands ($\boldsymbol{q^d} = (q_1^d, q_2^d, q_3^d)$) using the inverse kinematic model ($\boldsymbol{h(r)}$) implemented in the controller:

$$\boldsymbol{h}(\boldsymbol{r^d}) = \boldsymbol{q^d}, \tag{1}$$

The corresponding forward kinematic model maps back from the joint space to the task space ($\boldsymbol{g(q)} = \boldsymbol{h^{-1}(q)}$), and therefore:

$$\boldsymbol{g}(\boldsymbol{h}(\boldsymbol{r^d})) = \boldsymbol{g}(\boldsymbol{q^d}) = \boldsymbol{r^d} \tag{2}$$

Due to geometrical and non-geometrical errors, after executing $\boldsymbol{q^d}$ in the controller, the physical machine realizes the physical position $\boldsymbol{r^p}$, through the actual forward kinematics ($\boldsymbol{g^*(q)}$). This does hardly ever coincide with the corresponding digital position $\boldsymbol{r^d}$ in the same reference system:

$$\boldsymbol{g^*}(\boldsymbol{h}(\boldsymbol{r^d})) = \boldsymbol{g^*}(\boldsymbol{q^d}) = \boldsymbol{r^p} \neq \boldsymbol{r^d} \tag{3}$$

Here, $\boldsymbol{r^p}$ can be expressed as a function of both joint and task space variables. Since $\boldsymbol{h(r)}$, $\boldsymbol{g(q)}$ and $\boldsymbol{g^*(q)}$ are not available parametrically, and therefore cannot be modified, the goal is to determine the compensated joint vector $\boldsymbol{q_c^d}$ for which the actual forward model is:

$$\boldsymbol{g^*}(\boldsymbol{q_c^d}) = \boldsymbol{r_c^p} = \boldsymbol{r^d} \tag{4}$$

For this, first the workspace volume is discretized to a set of gridpoints G. Then the actual position is measured in the workspace as a function of the gridpoints in the model. Let $\boldsymbol{f_m(r)}$ be a discrete function $\boldsymbol{f_m}: \{\mathbb{R}^3 \to \mathbb{R}^3 | \boldsymbol{f_m}(\boldsymbol{r^d}) = \boldsymbol{r^p}\}$ based on the measurements in the gridpoints:

$$\boldsymbol{f_m}(\boldsymbol{r_i^d}) = \boldsymbol{r_i^p} = \boldsymbol{g^*}\left(\boldsymbol{h}(\boldsymbol{r_i^d})\right) \; \forall \, \boldsymbol{r_i^d} \in G \tag{5}$$

Let the compensation function $\boldsymbol{f_c(r)}$ be $\boldsymbol{f_c}: \{\mathbb{R}^3 \to \mathbb{R}^3 | \boldsymbol{f_c}(\boldsymbol{r^p}) = \boldsymbol{r^d}\}$ and let it be the least-square fit to $\boldsymbol{f_m^{-1}(r)}$. With this, using the desired task space position $\boldsymbol{r_c^p} = \boldsymbol{r^d}$, the corresponding compensated joint variables $\boldsymbol{q_c^d}$ and command position $\boldsymbol{r_c^d} = (x_c^d, y_c^d, z_c^d)$ can be calculated with $\boldsymbol{f_c}(\boldsymbol{r_d^p}) = \boldsymbol{f_c}(\boldsymbol{r^d}) = \boldsymbol{r_c^d}$, which results:

$$\boldsymbol{g^*}\left(\boldsymbol{h}\left(\boldsymbol{f_c}(\boldsymbol{r_c^p})\right)\right) = \boldsymbol{g^*}\left(\boldsymbol{h}(\boldsymbol{r_c^d})\right) = \boldsymbol{g^*}(\boldsymbol{q_c^d}) = \boldsymbol{r^d} \tag{6}$$

For evaluation and visualization purposes, the difference between the desired and compensated digital position (based on the measurement, without least-square fitting) is captured by:

$$\boldsymbol{\Delta r^d} = \boldsymbol{f_m^{-1}}(\boldsymbol{r^d}) - \boldsymbol{r^d} = \boldsymbol{r_m^d} - \boldsymbol{r^d} = (\Delta x^d, \Delta y^d, \Delta z^d) \tag{7}$$

2.1. Compensation in z direction

For the measurement of the z-directional tool center point (TCP) error, a digital indicator is fixed on the end-effector. Most digital indicators allow the saving of measurement data onto a computer drive, which makes synchronized data collection possible. Typically, these indicators have a couple tens of millimeters measurement range and 0.01-0.001 mm resolution, which is suitable for the accuracy of common manipulators.

The digital indicator is fixed with its spindle axis collinear with the z-axis of the TCP frame (see Figure 1(a)). In this setup, by touching the top plane of the worktable, the corresponding relative displacement of the indicator's contact point can be measured and stored.

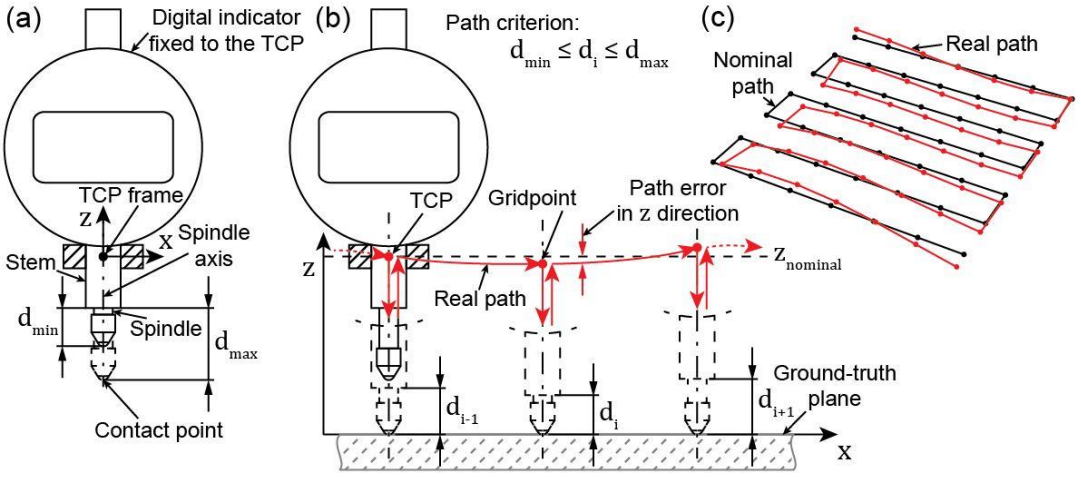

Figure 1. The digital indicator setup (a), arrangement of the z measurement process (b), and the corresponding path, without the vertical feed and retreat segments (c).

If the worktable does not allow proper scanning in the utilized workspace, a fixed reference plane parallel to the worktable can be used. However, the flatness and parallelism tolerances of the reference plane directly influence the calibration results.

For each gridpoint in G, the z coordinate of the end-effector is determined by measuring the relative displacement of the contact point. To scan the whole plane, a tool-path needs to be prepared. Following this path (see Figure 1(c)), the end-effector needs to stop at every defined gridpoint, wait for stabilization, as well as for measurement, before continuing the path. To avoid continuous sliding of the contact point, z-directional feed and retreat path segments are added in each gridpoint as shown in Figure 1(b).

Based on the gridpoints and the synchronized data collection, a map of z-directional displacements can be set up in a selected plane of the workspace volume using the x and y values from the robot controller. The resolution of the map depends on the number of gridpoints. With a denser grid, a more precise map can be achieved, however, the measurement time will also increase.

Consequently, in the first step, $z_c^d(\boldsymbol{q}(\boldsymbol{r}))$ needs to be determined. During measurement, the z-directional error is captured in the following way:

$$f_{m,z}(\boldsymbol{r_i^d}) = z_i^p(\boldsymbol{r_i^d}), \text{where } \boldsymbol{r_i^d} \in G \qquad (8)$$

To find the compensated control position, the inverse of this map is interpolated with a cubic polynomial (with z being constant):

$$f_{c,z}(\boldsymbol{r}) = \mathrm{p}_{z,1}x^3 + \mathrm{p}_{z,2}x^2y + \mathrm{p}_{z,3}xy^2 + \mathrm{p}_{z,4}y^3 + \mathrm{p}_{z,5}x^2 + \mathrm{p}_{z,6}xy + \mathrm{p}_{z,7}y^2 + \mathrm{p}_{z,8}x + \mathrm{p}_{z,9}y + \mathrm{p}_{z,10} \qquad (9)$$

That is, $f_{c,z}(\boldsymbol{r})$ is the least-square fit to $f_{m,z}^{-1}(\boldsymbol{r})$.

The interpolation function is further discussed in Section 4. At this point, in the selected *x-y* plane, the compensated control value z_c^d can be found as $f_{c,z}(\boldsymbol{r^d})$.

2.2. Compensation in x-y directions

In the second step, *x-y* measurement and compensation is carried out. Although sufficiently precise, mounting the digital indicator with its spindle axis precisely aligned to another axis of the TCP frame proves to be difficult in most cases. Instead, a low intensity laser pointer (unfocused) is mounted rigidly on the end-effector, aligned with the same *z*-axis. In addition, a 2D camera is fixed in eye-in-hand configuration. The camera needs to be calibrated for its intrinsic parameters (De la Escalera and Armingol, 2010), however the connection does not need to be rigid, and no hand-eye calibration is necessary. If observability allows, the camera could be fixed externally as well, still with no precisely known relation w.r.t. the machine. In this setup, a (printed) chessboard pattern is laid onto the surface subjected to *z* measurement. The square side length of the pattern is considered ground-truth. The measurement is based on the homography transformation (Bradski and Kaehler, 2000), i.e., by knowing the squares' side length, the location of the laser spot is determined w.r.t. the corners of the chessboard pattern.

Similarly to the *z*-axis calibration, the end-effector is moved along a tool-path, and in each gridpoint the motion is stopped to capture images of the laser spot on the chessboard pattern (see Figure 2). Stabilizing time is required here as well, however, no *z*-directional feed and retreat motion is necessary. Also, the camera needs to be set up in a way that the laser spot and all sides of its containing square always appear within the captured region.

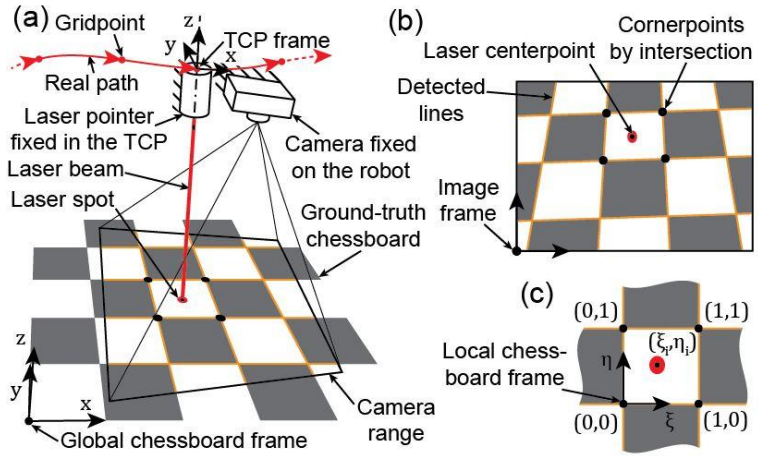

Figure 2. Arrangement of the *x-y* measurement (a), corresponding camera image (b) and the reprojected image (c).

Two consecutive images are captured at each gridpoint, with the laser turned on and off. Additionally, to further facilitate the cornerpoint detection, LED light sources are switched on whenever the laser is turned off, to provide a fairly homogeneous lighting setup. For consistent measurement, the automatic features of the camera are recommended to be turned off, including the brightness, white balance and focus.

First, the chessboard image is processed. To find the cornerpoints of chessboard patterns, a line detection-based approach is applied. After binarizing the image and applying edge detection, the sides of the squares are highlighted. Using a RANSAC-based fitting method (Choi *et al.*, 1997), the lines are found on the camera image, which unfold the chessboard corners by intersection.

Then, with the help of the homography transformation, the images are reprojected to eliminate the perspective distortion caused by the camera. Next, the laser spot is localized on the laser image. The laser spot can be easily found on the reprojected image via thresholding and centerpoint calculation, due to the high light intensity of the lasers. Finally, the results of the two images are overlaid, based on which the neighboring cornerpoints are determined, and the laser point is localized in the task space, w.r.t. the chessboard corners (see Figure 2(c)).

Following the path and the *x-y* controller coordinates synchronized with the measurement, the laser point can be determined w.r.t. the calibration board in each gridpoint (provided that the *x-y* error is smaller than the side length). From here, the error map can be set up using the measured error and controller values, similarly to the *z* error map, in both *x* and *y* direction. The *x*-directional measurement can be formulated as:

$$f_{m,x}\left(\boldsymbol{r_i^0}+\left(0,0,\Delta z_i\left(\boldsymbol{r_i^0}\right)\right)\right)=x_i\left(\boldsymbol{r_i^0}\right),\text{where } \boldsymbol{r_i^0}\in G \qquad (10)$$

The interpolation function is formed as in Equation (9). The *y*-directional compensation function is formulated just like in case of *x*. From here, the complete compensation function can be written as:

$$\boldsymbol{f_c}(\boldsymbol{r})=\left(f_{c,x}(\boldsymbol{r}),f_{c,y}(\boldsymbol{r}),f_{c,z}\left(\left(f_{c,x}(\boldsymbol{r}),f_{c,y}(\boldsymbol{r}),z\right)\right)\right) \qquad (11)$$

Note that the *z*-directional compensation needs to be found for the compensated *x* and *y* values. The tool-path segments can now be compensated in the controller, before applying the inverse kinematics.

3. Implementation

The proposed method was implemented and executed on an in-house developed and built, 3-DoF linear-delta type PKM (see Figure 3). It is a multi-purpose machine used for in-house projects, research and education. The PKM has a modular platform with different special tool holders, including a laser engraver, drawing tools and an entry-level milling spindle, among others. Most tasks, in which the machine is utilized, require offline programming and precise planar positioning, for which the original accuracy of the machine is not suitable. The accuracy of the PKM was improved using the proposed calibration method. The structure, control and kinematic model of the PKM is described in Anonymous, 2016.

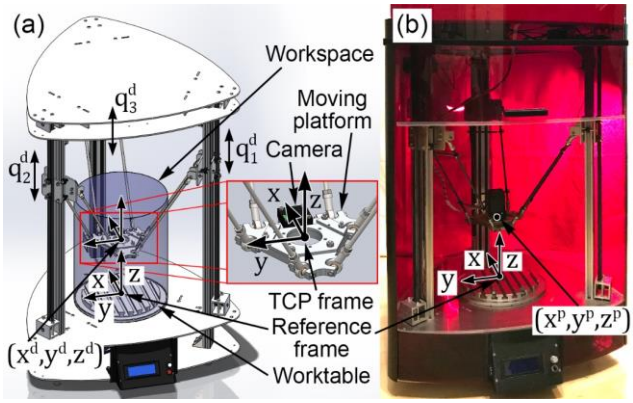

Figure 3. CAD design with main components and DoFs (a) and the actual the PKM equipped with a laser engraver (b).

3.1. Setup

Following the steps of the proposed method, two setups are necessary. First, the *z* measurement setup is prepared, starting with the installation of a glass sheet with the chessboard pattern. The chessboard pattern is printed on a vinyl layer, which is laid onto the glass sheet. This board is fixed on the machine table with a self-adhesive layer on the bottom of the glass sheet. Such fastening is sufficient, since the plate does not displace under the small acting normal force during measurement. Actually, this setup also corresponds to laser engraving and drawing operations, with an additional layer of cork sheet on top of the glass, and as such, functions as a worktable.

Next, a Mitutoyo ID-110M digital indicator is placed on the moving platform of the PKM. Using rapid prototyping, a clamp collar was created to fix the stem of the digital indicator concentrically to the *z*-axis of the TCP frame on one of the tool holder modules (see Figure 4(a)). The module was then fixed to the platform, and the indicator was connected to the controller for the synchronized data collection. With this, the mechanical setup for *z* measurement is ready.

A Raspberry Pi camera module is installed onto the moving platform and is connected to the controller by design, which is used for the *x*-*y* measurement. The camera is set up with an image resolution of 700x875, and automated features (mentioned in Section 2.2) turned off. The calibration board setup is not changed. However, the tool holder carrying the digital indicator is replaced. On another console created with rapid prototyping, the light sources are set up. This contains altogether 4 white LEDs and 2 laser diodes (pointers) with parallel axes, one in the center and another with an offset (see Figure 4(b)). The second laser pointer was installed for further experimental possibilities (e.g., measuring rotation around the *z*-axis). The light sources were then connected to controller outputs to realize synchronized switching.

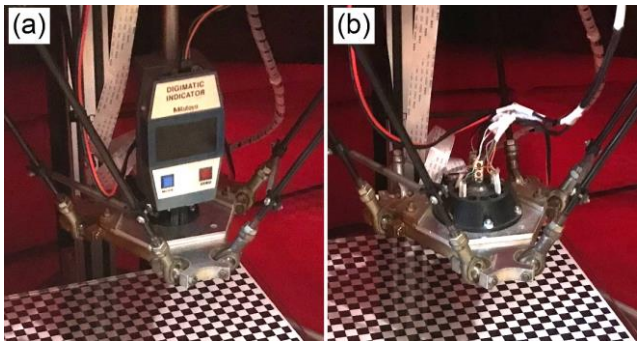

Figure 4. Tool holders for the *z* (a) and *x*-*y* measurements (b).

3.2. Calibration

The calibration was carried out based on a *z* and an *x*-*y* measurement session. In each session, 6 measurement cycles were carried out, 3 with forward and 3 with reverse path. For each gridpoint, the mean of the 6 measurement values was taken. The spacing of the grid was selected to be 5 mm, which resulted 2053 calibration gridpoints. A zigzag path was created for scanning the circle base of the workspace. The image-processing was carried out in Wolfram Mathematica 10 and the measurement and computation times are summarized in Table I.

Table I. Mean measurement and image-processing times for a single cycle of 2053 gridpoints (Intel I5-6440HQ CPU @ 2.60GHz computer under Windows 10).

Measurement time (*z*)	61 min
Measurement time (*x*-*y*)	58 min
Image processing time	23 min
Chessboard corner detection time	0.531 s/gridpoint
Laser centerpoint (x2) localization time	0.129 s/gridpoint

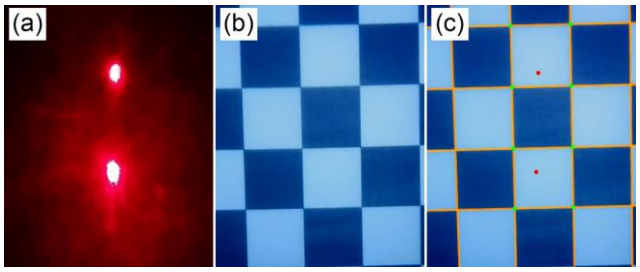

Figure 5. The captured laser image (a), the chessboard image (b), and the results mapped on the original image after image-processing (c).

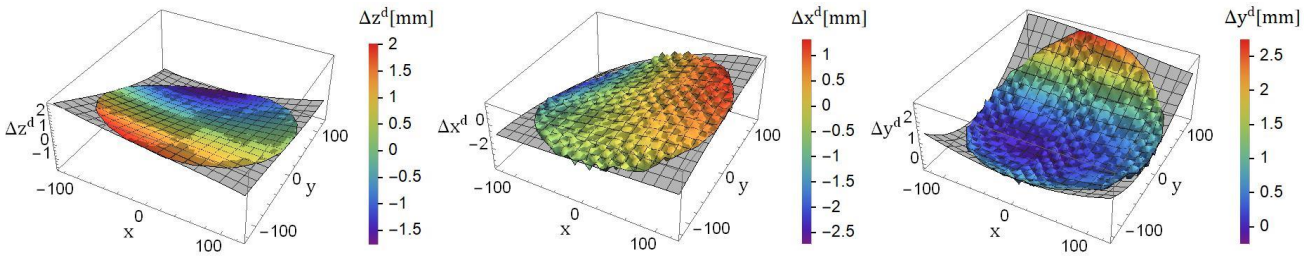

Figure 6. Measurement results before calibration, and the corresponding interpolation functions.

After the first *z* measurement session, the error map is prepared, with which the first *x-y* measurement session and image-processing are carried out. As an example, captured images for a single gridpoint are shown in Figure 5. At this point, the deviations in each direction $(\Delta x^d, \Delta y^d, \Delta z^d)$ can be plotted. To finalize the calibration, the *x-y* error maps are also prepared and implemented in the controller. The results of the sessions before calibration are shown in Figure 6, along with the relative interpolation functions (with gray). It is noted that for each result figure, instead of the point-like data, the results are presented with linear interpolation for better visibility. The interpolation function is shifted $(\boldsymbol{f_c}(\boldsymbol{r}) - \boldsymbol{r})$ for the same reason.

3.3. Verification

To evaluate the achieved results, *z* and *x-y* measurements were carried out after compensation in a similar manner as before calibration. The only difference was the halved (2,5 mm) spacing, resulting in 8161 measurement points. The deviation values after compensation $(\boldsymbol{\Delta \hat{r}^d})$ are shown in Figure 7.

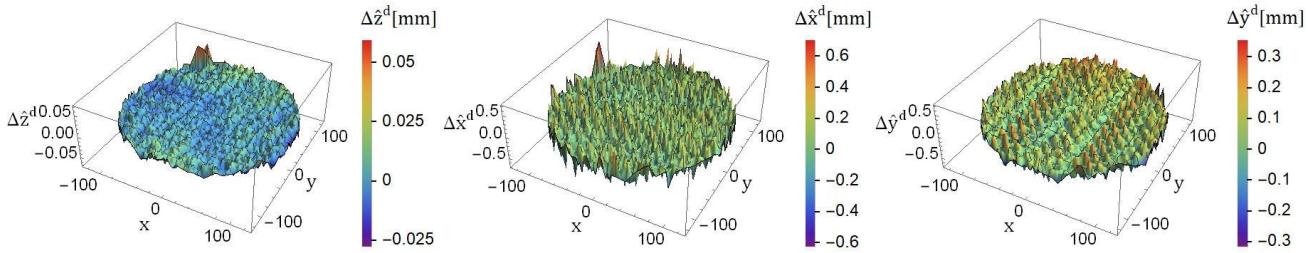

Figure 7. Measurement results after calibration.

Apart from measuring on a finer grid, the *x-y* calibration was further analyzed using an actual manufacturing operation of the PKM. Using the laser engraver tool, a square grid with 4 mm spacings was engraved onto a thin A4 size cardboard sheet. This grid was prepared based on the base circle of the workspace, and was slightly trimmed to fit onto the 210 mm width of the paper in the *y* direction, resulting in 2707 gridpoints. The engraving process was carried out two times, once with compensation and once without it. The sheets were digitalized using an image scanner with a 1200 dpi resolution, then the gridpoints were determined via image-processing. By comparing the nominal gridpoints (from the tool-path) with the scanned gridpoints, the deviation between the point-pairs could be identified. The verification results before $(\Delta x_v^d, \Delta y_v^d)$ and after calibration $(\Delta \hat{x}_v^d, \Delta \hat{y}_v^d)$ are shown in Figure 8 and Figure 9, respectively. Finally, the numerical results are summarized in Table II.

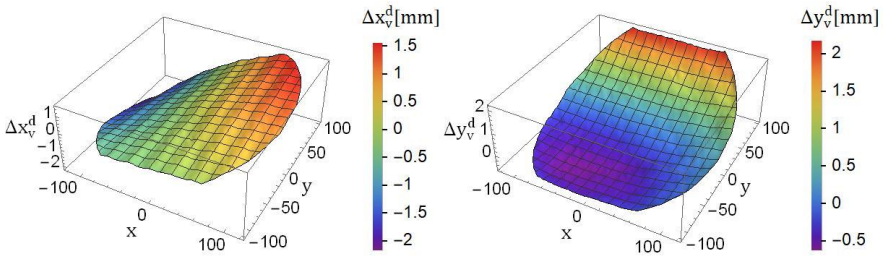

Figure 8. Verification results before calibration.

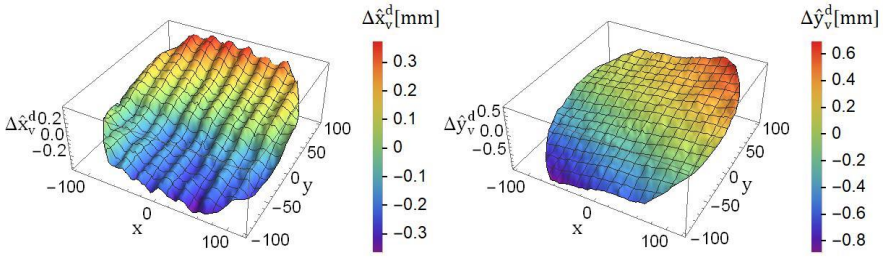

Figure 9. Verification results after calibration.

The $(\Delta x_v^d, \Delta y_v^d)$ results clearly resemble the $(\Delta x^d, \Delta y^d)$ ones, which shows the adequacy of the proposed measurement technique. The $(\Delta \hat{x}_v^d, \Delta \hat{y}_v^d)$ results show the combined inaccuracy of the chessboard pattern and the measurement technique. After checking the printed chessboard pattern, an approximately 3% shrinkage is observable along the *y*-axis, resulting in a noticeable global error.

Table II. Verification results.

	Digital indicator setup Δz^d [mm]	Camera-laser setup $(\Delta x^d, \Delta y^d)$ [mm]	Laser engraving setup $(\Delta x_v^d, \Delta y_v^d)$ [mm]
Mean abs. deviation before calib.	0.778	(0.665, 0.644)	(0.673, 0.598)
Max. abs. deviation before calib.	2.008	(2.732, 2.737)	(2.175, 2.165)
	$\Delta \hat{z}^d$ [mm]	$(\Delta \hat{x}^d, \Delta \hat{y}^d)$ [mm]	$(\Delta \hat{x}_v^d, \Delta \hat{y}_v^d)$ [mm]
Mean abs. deviation after calib.	0.005	(0.087, 0.062)	(0.143, 0.276)
Max. abs. deviation after calib.	0.059	(0.706, 0.353)	(0.372, 0.893)

As visible from both verification results in Table II, significant improvement is achieved with the proposed technique.

4. Discussion and work in progress

The improvement in the positioning accuracy is noticeable in each direction, in particular, the *z*-directional compensation is most convincing. It is important to note that due to the relative measurement technique (w.r.t. the chessboard), datum frame setup is necessary to align the frame origin and axes to the machine reference frame.

Although the *x*-*y* calibration also improves the accuracy significantly, the results require attention. In both *x* and *y* directions the results show a pattern of increased local change in the measurement data in form of bumps. These are measurement inaccuracies caused by the black-white transition of the chessboard pattern. Whenever the laser spot is in the vicinity of these edges, the measured value shifts towards the white square, as the black parts absorb the light much more, and the detected laser spot is deformed. This unfavorable phenomenon can be overcome while keeping the simple setup by changing the black-white color pair, i.e., using a modified chessboard pattern.

Once this error source is eliminated, different kinds of interpolation can be realized based on the 4 neighboring gridpoints instead of an overall interpolation function, which is more widespread in case of modeless approaches (Bai and Wang, 2019). This would result in a more accurate compensation and possibly faster computations with a tradeoff on the required memory.

For global calibration, when having the parametric error model (Huang, 2003), a model-based calibration is more suitable as less measurement points are necessary. The *x*-*y* measurement can be realized in different heights, which is only limited by the camera focus and proper observability of the laser spot on the chessboard. The *z* measurement can be repeated in different heights up to the measurement range of the digital indicator or with an additional ground-truth plane.

If the end-effector has no motion in the uncontrolled axes, precise collinearity of the measurement tools with the selected TCP axis is not crucial. The corresponding error is tackled during the datum frame setup, since it only results in a constant offset. However, if motion occurs in the uncontrolled DoFs (Huang, 2003), the collinearity error can have noticeable effect on the calibration results, which needs to be considered.

Lastly, the proposed method raises an opportunity for manufacturers, to equip machines with low-cost tools for measurement, calibration or compensation purposes.

5. Conclusion and future work

This paper presented a novel technique for modeless calibration of a PKM. With the help of a digital indicator, an eye-in-hand camera, a laser pointer and a chessboard pattern, 3D positioning errors of the PKM are compensated in the utilized workspace. The evaluated and verified proof of concept shows that significant improvement can be achieved in the positioning accuracy with the proposed method using low-cost tools and simple setups. This can make the proposed technique appealing for SMEs, as well as educational and research teams, with no expensive measuring devices or skilled workforce at their disposal. The method is most suitable for robotic tasks utilizing local regions of their workspace or machines with small workspace volume.

Future work includes the comparison of the model-based and modeless calibration processes with the proposed technique, and system improvement with a more suitable chessboard pattern to enhance *x*-*y* measurement precision. The application of additional laser pointers for more complete pose estimation is a further possible research topic.

Acknowledgement

This research has been partially supported by the Ministry for Innovation and Technology and the National Research, Development and Innovation Office within the framework of the National Lab for Autonomous Systems and partially by the ED_18-2-2018-0006 grant on "Research on prime exploitation of the potential provided by the industrial digitalisation".

References

Anonymous, (2016), Details omitted for double-blind reviewing.

Bai, Y. and Wang, D. (2019), "On the Comparison of Fuzzy Interpolations and Neural Network Fitting Functions in Modeless Robot Calibrations", *2019 IEEE International Conference on Fuzzy Systems (FUZZ-IEEE)*, pp. 1–6.

Bradski, G. and Kaehler, A. (2000), "OpenCV", *Dr. Dobb's Journal of Software Tools*, Vol. 3.

Cai, Y., Yuan, P. and Chen, D. (2018), "A Flexible Calibration Method Connecting the Joint Space and the Working Space of Industrial Robots", *Industrial Robot: An International Journal*, Vol. 45 No. 3, pp. 407–415.

Cao, C.-T., Do, V.-P. and Lee, B.-R. (2019), "A Novel Indirect Calibration Approach for Robot Positioning Error Compensation Based on Neural Network and Hand-Eye Vision", *Applied Sciences*, Vol. 9 No. 9, p. 1940.

Choi, S., Kim, T. and Yu, W. (1997), "Performance Evaluation of RANSAC Family", *Journal of Computer Vision*, Vol. 24 No. 3, pp. 271–300.

De la Escalera, A. and Armingol, J.M. (2010), "Automatic Chessboard Detection for Intrinsic and Extrinsic Camera Parameter Calibration", *Sensors*, Vol. 10 No. 3, pp. 2027–2044.

Dehghani, M., Ahmadi, M., Khayatian, A., Eghtesad, M. and Yazdi, M. (2014), "Vision-Based Calibration of a Hexa Parallel Robot", *Industrial Robot: An International Journal*, Vol. 41 No. 3, pp. 296–310.

Guo, Y., Yin, S., Ren, Y., Zhu, J., Yang, S. and Ye, S. (2015), "A Multilevel Calibration Technique for an Industrial Robot With Parallelogram Mechanism", *Precision Engineering*, Vol. 40, pp. 261–272.

Huang, T. (2003), "Kinematic Calibration of a Class of Parallel Kinematic Machines (PKM) With Fewer Than Six Degrees of Freedom", *Science in China Series E*, Vol. 46 No. 5, pp. 515–526.

Jiang, Y., Huang, X. and Li, S. (2016), "An On-Line Compensation Method of a Metrology-Integrated Robot System for High-Precision Assembly", *Industrial Robot: An International Journal*, Vol. 43 No. 6, pp. 647–656.

Li, W., Cao, G., Sun, J., Liang, Y. and Huang, S. (2017), "A Calibration Algorithm of the Structured Light Vision for the Arc Welding Robot", *2017 14th International Conference on Ubiquitous Robots and Ambient Intelligence (URAI)*, pp. 481–483.

Liao, S., Zeng, Q., Ehmann, K.F. and Cao, J. (2020), "Parameter Identification and Nonparametric Calibration of the Tri-Pyramid Robot", *IEEE/ASME Transactions on Mechatronics*, Vol. 25 No. 5, pp. 2309–2317.

Majarena, A.C., Santolaria, J., Samper, D. and Aguilar, J.J. (2010), "An Overview of Kinematic and Calibration Models Using Internal/External Sensors or Constraints to Improve the Behavior of Spatial Parallel Mechanisms", *Sensors*, Vol. 10 No. 11, pp. 10256–10297.

Mekid, S. and Ogedengbe, T. (2010), "A Review of Machine Tool Accuracy Enhancement Through Error Compensation in Serial and Parallel Kinematic Machines", *International Journal of Precision Technology*, Vol. 1 No. 3–4, pp. 251–286.

Meng, Y. and Zhuang, H. (2007), "Autonomous Robot Calibration Using Vision Technology", *Robotics and Computer-Integrated Manufacturing*, Vol. 23 No. 4, pp. 436–446.

Mooring, B., Roth, Z.S. and Driels, M.R. (1991), *Fundamentals of Manipulator Calibration*, Wiley, New York.

Nubiola, A. (2014), *Contribution to Improving the Accuracy of Serial Robots*, PhD Thesis, École de Technologie Supérieure.

Özgüner, O., Shkurti, T., Huang, S., Hao, R., Jackson, R.C., Newman, W.S. and Çavuşoğlu, M.C. (2020), "Camera-Robot Calibration for the Da Vinci Robotic Surgery System", *IEEE Transactions on Automation Science and Engineering*, Vol. 17 No. 4, pp. 2154–2161.

Patel, D., Lienenlüke, L., Storms, S., Brecher, C. and Wied, J. (2019), "Improving the Absolute Accuracy by Online Interpolation Technique of Industrial Robots", *IOP Conference Series: Materials Science and Engineering*, Vol. 575.

Wang, D. and Bai, Y. (2012), "Calibration of Stewart Platforms Using Neural Networks", *2012 IEEE Conference on Evolving and Adaptive Intelligent Systems*, pp. 170–175.

Zhuang, H. and Roth, Z.S. (1996), *Camera-Aided Robot Calibration*, CRC press, Boca Raton.